

## MOMENTUM AND HEAT TRANSFER ACROSS FREELY-FALLING TURBULENT LIQUID FILMS

I. A. MUDAWWAR

School of Mechanical Engineering, Purdue University, West Lafayette, IN 47907, U.S.A.

M. A. EL-MASRI

Department of Mechanical Engineering, Massachusetts Institute of Technology, Cambridge,  
MA 02139, U.S.A.

(Received 24 April 1985; in revised form 31 December 1985)

**Abstract**—This work centers on the transport processes in turbulent liquid films undergoing heating or surface evaporation. A new semi-empirical turbulence model is presented. It consists of a single continuous eddy-viscosity profile which spans the entire liquid layer. Numerical calculations reveal good agreement with experimental data for freely-falling films. It was found that it is impossible to obtain universal correlations for different fluids in terms of Reynolds and Prandtl numbers alone since the heat transfer data display strong dependence on the Kapitza number below  $Re = 10,000$ . The Kapitza number accounts for the effects of surface tension and viscosity on the turbulence structure near the free surface of the film. Turbulent-film correlations similar to those used in conventional internal or external flows are recommended for higher Reynolds numbers.

### 1. INTRODUCTION

Modeling of turbulent liquid films has been the target of extensive research spanning the last six decades. Detailed understanding of the film transport processes was of paramount importance for evaluating the performance of various heat-exchanger configurations.

Nusselt (1916) solved the momentum and energy equations for smooth laminar freely-falling liquid films by neglecting the effects of interfacial waves or vapor shear stress. The importance of surface waves on the transport processes in laminar films has been stressed by several investigators. The works by Benjamin (1957), Hanratty & Hershman (1961), Whitaker (1964), Kapitza (1965), Massot *et al.* (1966), Gollan & Sideman (1969) and Berbente & Ruckenstein (1968) are only a few examples. Theoretical models by these authors led to lower estimates of the film thickness compared to Nusselt's solution. It is interesting to note that many of these analyses define the wave characteristics as functions of the Reynolds number ( $Re$ ) and an additional dimensionless parameter, namely the Kapitza number ( $Ka$ ), defined by

$$Ka \equiv \frac{\mu^4 g}{\rho \sigma^3}, \quad [1]$$

where  $g$  is the acceleration due to gravity, and  $\mu$ ,  $\rho$  and  $\sigma$  are the viscosity, density and surface tension of the liquid, respectively.

Wave effects were studied experimentally by various investigators. The works of Brauer (1956), Feind (1960) and Portalski (1963), are a few examples of these efforts. Changes in the wave pattern as well as the average film thickness were used to define the transitional characteristics of the film with increasing  $Re$ . Smooth film flows were obtained only for very low  $Re$ . As  $Re$  was increased, short waves were reported to traverse the surface at relatively high speeds (up to four times the average film speed). With further increases in  $Re$ , the wave speed approached the average film speed. Transition to turbulent flow was also characterized by a significant increase in the average thickness beyond Nusselt's prediction.

The developing effects of falling-film waves were studied experimentally by Portalski & Clegg (1972) and Salazar & Marschall (1978). Their data reveal that no fully-developed wave characteristics could be achieved with turbulent films. More recent data, by

Kirkpatrick (1980) and Takahama & Kato (1980), show that, unlike the case of laminar films, turbulent wave activity is characterized by very long waves (wavelengths were 2 orders of magnitude greater than the average film thickness). These sources also indicate that the ratio of maximum-to-minimum thickness actually increases with  $Re$  and with distance. This fact demonstrates the difficulty of modeling any wave activity in turbulent films. For this reason, smooth-surface models have been employed to predict mass, momentum and energy transport across liquid films. Smooth-surface assumptions can only be justified by the long waves that prevail in turbulent flows. Of more importance for modeling, however, is the turbulence structure across the film, and its impact on the film transport processes. Statistical studies on the wave characteristics of falling films, such as those of Chu & Dukler (1974) and Kirkpatrick (1980), indicate the presence of at least two classes of random waves: large inertia-dominated waves whose amplitude is comparable to the average thickness of the film; and small waves which cover the surface of the large waves as well as the substrate film that exists between large waves. The amplitude of the second class of waves was typically of the order of 0.05 mm for water films in the transition region ( $Re = 1600$ ). There was also some speculation about the existence of much smaller capillary waves whose characteristics were beyond the reach of available film-thickness measurement devices. Surface tension forces resist any tendency of deformation by the film free surface. This is particularly the case with small ripples, where the importance of surface tension forces overshadows those of other driving forces associated with the formation of large waves. During the transition from wavy-laminar to turbulent film flow, velocity fluctuations are generated within the film. These fluctuations are completely suppressed at the solid wall. The free surface of the film can deform under the action of inertia and gravity forces. The amplitude and curvature of the smallest deformations is governed by surface tension forces. Thus deformations caused by turbulent velocity fluctuations are totally damped by surface tension. As turbulent eddy activity is suppressed at the free surface, viscous forces play a significant role in that region, creating a free-surface boundary layer within the film similar to the one associated with the solid wall. Thus, the extent of this surface layer depends on  $Ka$ , defined in [1].

Based on the above discussion, one can draw the general conclusion that transition to turbulent film flow is a highly complicated phenomenon. Furthermore, turbulence models developed for highly-turbulent flows should be modified to account for changes in wave activity associated with transition from wavy-laminar to turbulent-film flow. This goal can be achieved through empirical correlations which account for the  $Ka$  effect. Unfortunately, only a few reliable experimental studies are available in the literature, particularly with respect to heat transfer coefficients of turbulent freely-falling films.

In a gravity-driven film, the velocity  $u$ , and temperature  $T$ , at a distance  $y$  from the solid wall (see figure 1) are obtained from the momentum equation and the heat flux distribution across the film:

$$1 - \frac{y^+}{\delta^+} = \left(1 + \frac{\epsilon_M}{\nu}\right) \frac{du^+}{dy^+} \quad [2]$$

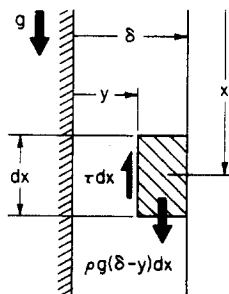


Figure 1. Force balance on a fluid element in a freely-falling film.

and

$$\frac{q}{q_w} = \frac{1}{\text{Pr}} \left( 1 + \frac{\text{Pr}}{\text{Pr}_T} \cdot \frac{\epsilon_M}{\nu} \right) \frac{\partial T^+}{\partial y^+}, \quad [3]$$

where  $\epsilon_M/\nu$  is the eddy-to-kinematic viscosity ratio,  $\text{Pr}$  and  $\text{Pr}_T$  are the Prandtl number and the turbulent Prandtl number,  $q$  and  $q_w$  are the local heat flux normal to the wall and the wall flux, respectively.

The variables of [2] and [3] are nondimensionalized in terms of the friction velocity  $u_*$  as follows:

$$u_* \equiv \sqrt{\frac{\tau_w}{\rho}} = \sqrt{g\delta}, \quad [4]$$

$$y^+ \equiv \frac{u_* y}{\nu}, \quad [5]$$

$$u^+ \equiv \frac{u}{u_*}, \quad [6]$$

$$\delta^+ \equiv \frac{u_* \delta}{\nu} \quad [7]$$

and

$$T^+ \equiv \frac{\rho c_p u_* (T_w - T)}{q_w}, \quad [8]$$

where  $\delta$  is the film thickness,  $\tau_w$  is the wall shear stress,  $c_p$  is the specific heat at constant pressure and  $T_w$  is the wall temperature.

Most of the effort in modeling turbulent liquid films centers on the determination of the eddy-viscosity profile across the film. The film thickness is evaluated from [2], and mass conservation. Predictions based on [2] are more sensitive to the accuracy of the eddy-viscosity distribution in the vicinity of the solid wall (i.e. where  $y^+/\delta^+ \ll 1$ ). Near the free surface, however, the l.h.s. of [2] approaches zero and changes in  $\epsilon_M/\nu$  would not yield a significant effect on  $\delta$ . The same could be said about the heat transfer coefficient across fully-developed nonevaporating films. In this particular case, the l.h.s. of [3] decreases monotonically from unity at the solid wall ( $y^+ = 0$ ) until it approaches zero at the free surface, since all the energy supplied at the solid wall is absorbed by the film in the form of sensible heat. This is not the case, however, with evaporation or condensation, where the heat flux is conserved across the film until it is released at the free surface in the form of latent heat. The l.h.s. of [3] is fixed at unity and the temperature profile becomes sensitive to the detailed variation of  $\epsilon_M/\nu$  near the solid wall as well as the free-surface region. It follows that an approximate eddy-viscosity profile which fails to account for surface damping might still be successful in predicting the film thickness and the heat transfer coefficient in a nonevaporating liquid film. Using the same profile for evaporating films, however, might substantially underestimate the temperature gradient across the film. Most of the error in earlier semi-empirical estimates of the heat transfer coefficient resulted from neglecting the effects of surface tension and viscous forces at the free surface. These forces represent a major suppressant of turbulent activity in that region.

Early turbulent-film models, like those of Seban (1954) and Rohsenow *et al.* (1956), assumed a universal velocity-profile distribution typical of flat-plate boundary layers, in addition to Reynolds' analogy between momentum and heat transfer (i.e.  $\text{Pr}_T = 1$ ). Dukler (1960), on the other hand, used the Deissler equation for eddy viscosity in the region  $0 \leq y^+ \leq 20$ , and the von Karman equation through the rest of the film. According to Lee (1964), however, Dukler's analysis suffers from physical inconsistencies resulting from the discontinuity of the eddy-viscosity profile. Dukler's analysis was used later by Skelland & Popadic (1975) for modeling pseudoplastic liquids. Iribarne *et al.* (1967), on the other

Table 1. Turbulence models of freely-falling films

Authors	Model
Dukler (1960)	$\frac{\epsilon_M}{\nu} = n u^+ \left[ 1 - \exp(-2 u^+) \right]$ $\frac{\epsilon_M}{\nu} = K \left[ \frac{du^+}{dy^+} \right]^3 / \left[ \frac{d^2 u^+}{dy^{+2}} \right]^2$ $Pr_T = 1.0$
Iribarne et al. (1967)	$\frac{\epsilon_M}{\nu} = \frac{K}{12} \left[ e^{Ku^+} - 1 - Ku^+ - \frac{(Ku^+)^2}{2!} - \frac{(Ku^+)^3}{3!} \right]$ $K = 0.4$
Kunz & Yezunits (1967)	$\frac{\epsilon_M}{\nu} = -\frac{1}{2} + \frac{1}{2} \sqrt{1 + 4K^2 y^+} \left[ 1 - \exp\left(-\frac{y^+}{A^+}\right) \right]^2 \left(1 - \frac{y^+}{A^+}\right)$ $Pr_T = 0.667 \exp\left\{ \left( \frac{\epsilon_M}{\nu} \cdot Pr \right) 0.64 \right\} \quad (\text{liquid metals})$ $K = 0.4$
Mills & Chung (1973)	$\frac{\epsilon_M}{\nu} = -\frac{1}{2} + \frac{1}{2} \sqrt{1 + 4K^2 y^+} \left[ 1 - \exp\left(-\frac{y^+}{A^+}\right) \right]^2$ $y_i^+ \leq y^+ \leq 1 \quad \frac{\epsilon_M}{\nu} = 6.47 \times 10^{-7} Ka^{1/3} \frac{Re^{1.678}}{\delta^{+2/3}} (\delta^+ - y^+)^2$ $Pr_T = 0.9$ $K = 0.4; A^+ = 26$

$$0 \leq y^+ < 0.6 \delta^+ \quad \frac{c_M}{v} = -\frac{1}{2} + \frac{1}{2} \sqrt{1 + 4K^2 y^{+2} \left[ 1 - \exp \left\{ -\frac{y^+ \left(1 - \frac{y^+}{\delta^+}\right)^{1/2}}{A^+} \right\} \right]^2 \left(1 - \frac{y^+}{\delta^+}\right) \exp \left(-3.32 \frac{y^+}{\delta^+}\right)}$$

$$0.6 \delta^+ \leq y^+ \leq \delta^+ \quad \frac{c_M}{v} = \frac{c_M}{v} \Big|_{y^+ = 0.6 \delta^+}$$

Limberg (1973)

$$Pr_T = 0.89$$

$$K = 0.41; A^+ = 25.1$$

$$0 \leq y^+ \leq \delta^+ \quad \frac{c_M}{v} = -\frac{1}{2} + \frac{1}{2} \sqrt{1 + 4K^2 y^{+2} \exp \left\{ \frac{-2 \left(1 - \frac{y^+}{25}\right)^{G_1}}{G_2} \right\} \left(1 - \frac{y^+}{\delta^+}\right)}$$

Gimbutis (1974)

$$Pr_T = 0.9$$

K = 0.4; G<sub>1</sub> and G<sub>2</sub> are empirical functions of Re

$$0 \leq y^+ < 0.6 \delta^+ \quad \frac{c_M}{v} = -\frac{1}{2} + \frac{1}{2} \sqrt{1 + 4K^2 y^{+2} \left[ 1 - \exp \left\{ -\frac{y^+ \left(1 - \frac{y^+}{\delta^+}\right)^{1/2}}{A^+} \right\} \right]^2 \left(1 - \frac{y^+}{\delta^+}\right) \exp \left(-3.32 \frac{y^+}{\delta^+}\right)}$$

$$0.6 \delta^+ \leq y^+ \leq y^*_+ \quad \frac{c_M}{v} = \frac{c_M}{v} \Big|_{y^+ = 0.6 \delta^+}$$

Seban & Faghri (1976)

$$\frac{c_M}{v} = 6.47 \times 10^{-4} ka^{1/3} \frac{Re^{1.678}}{\delta^{+2/3}} (\delta^+ - y^+)^2$$

$$Pr_T = 0.9$$

$$Pr_T = 0.9 \frac{1 - \exp(-y^+/A^+)}{1 - \exp\left(-\frac{y^+ Pr_T^{1/2}}{B^+}\right)}; B^+ = f(Pr) \text{ (Habib & Na (1974))}$$

$$K = 0.40; A^+ = 25.1$$

y<sub>+</sub><sup>\*</sup> defines the extent of the surface region eddy viscosity equation necessary to give within 10 percent the absorption coefficient measured by Lamourelle & Sandall (1972) at their lowest Schmidt number, 140.

continued

Table 1—Continued

Authors	Model
Hubbard, Mills & Chung (1976)	$\frac{\epsilon_M}{v} = -\frac{1}{2} + \frac{1}{2} \sqrt{1 + 4K^2 y^+} \left[ 1 - \exp\left(-\frac{y^+}{A^+}\right) \right]^2 \left(1 - \frac{y^+}{\delta^+}\right)$
	$\frac{\epsilon_M}{v} = \frac{8.13 \times 10^{-17}}{Ka} \cdot \frac{Re^{2m}}{\delta^+ + 273} (\delta^+ - y^+)^2$ <p> <math>Pr_T = 0.9, 1.0, 1.1</math>  <math>K = 0.4; A^+ = 26; m = 6.95 \times 10^{-2} / 2, v \text{ in m}^2/\text{s}</math> </p>
Mudawwar & El-Masri	$\frac{\epsilon_M}{v} = -\frac{1}{2} + \frac{1}{2} \sqrt{1 + 4K^2 y^+} \left(1 - \frac{y^+}{\delta^+}\right)^2 \left[ 1 - \exp\left\{-\frac{y^+}{26} \left(1 - \frac{y^+}{5}\right)^{1/2} \left(1 - \frac{0.865 Re^{1/2}}{\delta^+} \right)\right\} \right]^2$
	<p>Heating: <math>Re_{crit} = \frac{97}{Ka^{0.1}}</math></p>
	<p>Evaporation: <math>Re_{crit} = \frac{0.04}{Ka^{0.37}}</math></p>
	$Pr_T = 1.4 \exp\left(-15 \frac{y^+}{\delta^+}\right) + 0.66$
	<p><math>K = 0.40; A^+ = 26</math></p>

hand, adopted the Spalding (1961) velocity-profile distribution to investigate diffusion-controlled electrolytic mass transfer between a falling film and a wall. Details of these models and others are given in table 1.

The Van Driest (1956) equation for  $\epsilon_M/\nu$ , first introduced for pipe flows, was used extensively during the last two decades for solving the turbulent-film transport equations. This was achieved by modifying the turbulent-sublayer linear mixing length functions with the exponential damping coefficient  $[1 - \exp(-y^+/A^+)]$ , which forces the mixing length to zero at the wall,  $A^+$  being an empirical constant. Van Driest's turbulence model was used by several investigators, such as Kunz & Yerazunis (1967) and Brumfield & Theofanous (1976), for calculating heat transfer coefficients for falling films as well as for two-phase flow in pipes. It should be noted, however, that this model applies only for the solid wall region, and does not provide any information about the free surface of the film.

In more recent years, modeling efforts have been concentrated on the bulk and free-surface regions of the film. In these models, the Van Driest function was still utilized for characterizing the wall region. The bulk and free-surface regions, however, were accounted for by introducing different functions for eddy viscosity. Limberg (1973), for example, assumed direct analogy with pipe flow eddy profiles. However, when the data of Chun & Seban were first published in 1971, it was discovered that all previous models had tended to overestimate the evaporation heat transfer coefficient. This fact motivated several investigators to correct the eddy-viscosity profile by accounting for turbulent suppression near the free surface of the film. The works of Mills & Chung (1973), Hubbard *et al.* (1976) and Seban & Faghri (1976), represent major efforts in that direction. In these models, surface damping was accounted for by analogy with mass species diffusion resulting from gas absorption into turbulent liquid films. By assuming a fixed turbulent Schmidt number, they used the mass transfer correlations of Lamourelle & Sandall (1972) and Chung & Mills (1974), for gas absorption into turbulent films. The complete eddy profile was constructed of discontinuous functions which accounted for the wall and surface regions separately. Similar assumptions were later used by Blangetti & Schlunder (1978) for shear-driven flows, and Yih & Chen (1982) for thermal entrance-region calculations.

Experimentally measured profiles for  $\epsilon_M$  or  $\epsilon_H$  were recently published by Ueda *et al.* (1977) for open-channel flows. Their experimental setup consisted of a 5-m long, 5.5-cm high and 49.5-cm wide test channel. The bottom wall was thermally insulated while the free surface was subjected to a high radiant heat flux. Their experimental results reveal that the eddy diffusivity reaches a maximum value in the core regions and drops to zero at the surface. The variation of  $\epsilon_M$  was fitted by the following equation:

$$\frac{\epsilon_M}{\nu} = Ky^+ \left( 1 - \frac{y^+}{\delta^+} \right), \quad [9]$$

where  $K$  is Von Karman's constant.

Ueda *et al.* (1977) attempted to explain these measurements by the interaction of surface waves with internal turbulent eddies. Calculations based on their model, however, exhibit some departure from data near the free surface.

In the following sections, we shall introduce a new semi-empirical turbulent-film model. Numerical results based on this model will be compared with various falling-film data.

## 2. PROPOSED TURBULENCE MODEL FOR LIQUID FILMS

In the proposed model we are going to introduce the following correlations to establish semi-empirical eddy-viscosity and  $Pr_T$  profiles.

(1) The variation of eddy viscosity in the bulk region is obtained from the experimental profile of Ueda *et al.* (1977):

$$\frac{\epsilon_M}{\nu} = l^{+2} \frac{du^+}{dy^+} = Ky^+ \left( 1 - \frac{y^+}{\delta^+} \right), \quad [10]$$

which is combined with [2] (for  $\epsilon_M/\nu \gg 1$ ) to obtain the mixing-length profile

$$l^+ = \frac{u_* l}{\nu} = Ky^+ \sqrt{1 - \frac{y^+}{\delta^+}} \quad [11]$$

This profile applies strictly in the turbulent sublayer which engulfed most of the water layer in Ueda's experiment. Equation [10] was selected for the proposed model because it was based on experimental measurements in a free-surface liquid layer. Such measurements have not yet been obtained with thin falling films.

(2) The viscous sublayer is accounted for by introducing the Van Driest (1956) damping function  $D$  to the turbulent mixing length, i.e.

$$l^+ = Ky^+ D \sqrt{1 - \frac{y^+}{\delta^+}} \quad [12]$$

$$\frac{\epsilon_M}{\nu} = K^2 y^{+2} D^2 \left(1 - \frac{y^+}{\delta^+}\right) \frac{du^+}{dy^+} \quad [13]$$

The above equations, therefore, apply throughout the liquid layer. Combining these equations with [2], we obtain the following eddy-diffusivity distribution function:

$$\frac{\epsilon_M}{\nu} = \frac{\sqrt{1 + 4K^2 y^{+2} \left(1 - \frac{y^+}{\delta^+}\right)^2 D^2 - 1}}{2} \quad [14]$$

(3) According to Kays (1972, 1980), the most complete Van Driest damping function has the form

$$D = 1 - \exp \left[ -\frac{y^+}{26} \left(1 - \frac{y^+}{\delta^+}\right)^{1/2} \cdot X_{\text{lam}} \right]; \quad [15]$$

$X_{\text{lam}}$  being a laminarization parameter which accounts for the influence of the free stream pressure gradient  $dP/dx$  on Van Driest's function. Based on a large number of flat-plate boundary-layer experiments performed at Stanford University, Kays obtained the following correlation for the laminarization parameter:

$$X_{\text{lam}} = 1 + 30.18 \left[ \frac{\mu \left(\frac{dP}{dx}\right)}{\rho^{1/2} \tau w^{3/2}} \right] \quad [16]$$

Unlike the Stanford experiments, however, freely-falling liquid films are driven by the gravitational body force. Replacing  $dP/dx$  in [16] by  $-\rho g$ , the laminarization parameter reduces to the following form:

$$X_{\text{lam}} = 1 - \frac{30.18}{\delta^+} \quad [17]$$

The significance of this parameter is that it completely suppresses turbulent activity as  $\delta^+$  approaches the value 30.18. Below this constant value, [17] is no longer applicable and the flow becomes completely laminar. Since liquid-film laminarization is significantly affected by wave activity and surface tension forces (in contrast to internal or external turbulent boundary-layer flows), the constant of [17] should be replaced in the case of falling films by a parameter which accounts for these effects. Equation [17] could then be written in the following form:

$$X_{\text{lam}} = 1 - \frac{\delta_{\text{crit}}^+}{\delta^+} \quad [18]$$

where

$$\delta_{crit}^+ = 0.865 Re_{crit}^{1/2}. \tag{19}$$

Equation [19] is simply the Nusselt thickness for laminar freely-falling films.

Equation [18] suggests that as Re approaches its transition (or critical) limit,  $X_{lam}$  will tend to zero, and the flow will become laminar.  $Re_{crit}$  for liquid films is thus a function of Ka (or surface tension parameter). In the heat transfer literature, investigators have relied on heat transfer data to correlate  $Re_{crit}$ , especially for high Pr liquids which exhibit more pronounced variations with Re. In the present analysis,  $Re_{crit}$  is defined as an "effective transitional" Re which is correlated from  $h^*$  vs Re experimental plots by the intersection of Nusselt's laminar equation with the best-fitted line for experimental data in the fully-turbulent regime (see figure 2). This procedure completely disregards the intermediate gradual transitions between the limiting regimes.  $Re_{crit}$  is correlated from Wilke's (1962) data for heated or isothermal films, and Chun & Seban's (1971) data for evaporating films:

$$\text{heating,} \quad Re_{crit} = \frac{97}{Ka^{0.1}} \tag{20a}$$

and

$$\text{evaporation,} \quad Re_{crit} = \frac{0.04}{Ka^{0.37}} \tag{20b}$$

The range of experimental conditions of Wilke and of Chun & Seban, as well as the base conditions for our numerical solutions are given in table 2.

The completely eddy-viscosity profile ultimately reduces to the following form:

$$\frac{\epsilon_M}{\nu} = -\frac{1}{2} + \frac{1}{2} \sqrt{1 + 4K^2 y^{+2} \left(1 - \frac{y^+}{\delta^+}\right)^2 \left\{ 1 - \exp \left[ -\frac{y^+}{26} \left(1 - \frac{y^+}{\delta^+}\right)^{1/2} \left(1 - \frac{0.865 Re_{crit}^{1/2}}{\delta^+}\right) \right] \right\}^2}. \tag{21}$$

Figure 3 shows a comparison between our predictions and some of the models discussed in the previous section. These plots are for evaporating freely-falling water films at 100°C. All these models tend to converge in the vicinity of the wall. Most of the previous models, however, tend to reduce eddy viscosity in the bulk and free-surface regions by two or more discontinuous functions. Furthermore, many earlier models (see table 1) assume that the eddy-viscosity profile is the same for the near transitional region ( $Re < 10^4$ ) and for the fully-turbulent region. The laminarization term of the present model relaxes this constraint and accounts for the variation of the turbulence structure with Re. This term is very important below  $Re = 10^4$ , yet it becomes insignificant for highly-turbulent flows ( $X_{lam} \rightarrow 1$  in [18]), where the modified Van Driest function becomes independent of the film Re like earlier models.

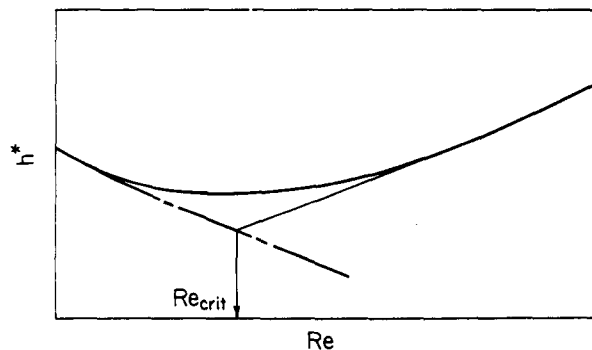


Figure 2. Method of correlating  $Re_{crit}$  for freely-falling films. —, Experimental data; ----, Nusselt's equation.

Table 2.  $Re_{crit}$ -values

Wilke's Data (Heating) (1960)					
Fluid	T(°C)	P(atm)	Pr	Ka	$Re_{crit}$
water	30	1	5.4	$1.15 \times 10^{-11}$	1200
water/ethyl-ene glycol	30	1	9.4	$6.7 \times 10^{-11}$	1000

Chun & Seban's Data (Evaporation) (1971)					
Fluid	$T_{sat}$ (°C)	$P_{sat}$ (atm)	Pr	Ka	$Re_{crit}$
water	28.3	0.038	5.7	$1.19 \times 10^{-11}$	440
water	100	1	1.77	$0.0314 \times 10^{-11}$	1700

Conditions Used in Numerical Calculations (Heating)					
Fluid	T(°C)	P(atm)	Pr	Ka	$Re_{crit}$
water	20	1	6.96	$2.55 \times 10^{-11}$	1112
water	50	1	3.56	$2.82 \times 10^{-12}$	1386
water	100	1	1.76	$3.15 \times 10^{-13}$	1726
water	150	1	1.148	$1.01 \times 10^{-13}$	1934
water	200	1	0.911	$6.76 \times 10^{-14}$	2013

Conditions Used in Numerical Calculations (Evaporation)					
Fluid	$T_{sat}$ (°C)	$P_{sat}$ (bar)	Pr	Ka	$Re_{crit}$
water	20	0.0234	6.96	$2.55 \times 10^{-11}$	332
water	99.6	1	1.75	$3.15 \times 10^{-13}$	1690
water	151.8	5	1.13	$1.01 \times 10^{-13}$	2573
water	179.9	10	0.98	$7.64 \times 10^{-14}$	2853

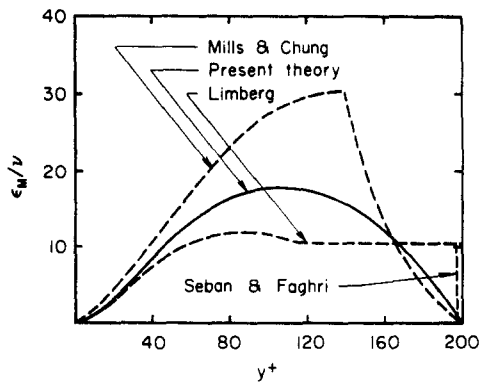


Figure 3. Comparison of the present theory with various models for the eddy-viscosity distribution across a vertical evaporating water film at 100°C ( $\delta^+ = 200$ ).

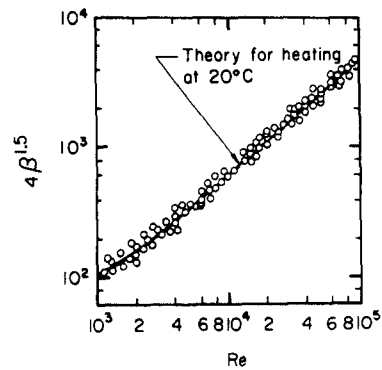


Figure 4. Comparison of calculated film thickness with various Russian data presented in Gimbutis' paper.

(4) The  $Pr_T$  profile is correlated from the experimental data of Ueda *et al.* (1977):

$$Pr_T = 1.4 \exp\left(-15 \frac{y^+}{\delta^+}\right) + 0.66. \quad [22]$$

This equation is based on water data at 50–58°C ( $Pr \approx 3$ ). Nevertheless, the authors have extended its use for other liquids and temperatures. This assumption could be justified by the fact that the effect of  $Pr$  on  $Pr_T$  is negligible in the range  $0.5 < Pr < 5$  in most  $Pr_T$  models. This conclusion is very well manifested by the close agreement between [22] and the experimental results of Abbrecht & Churchill (1960) for a fully-developed pipe flow of air ( $Pr = 0.7$ ) at  $Re = 15,000$  and  $65,000$ .

It should be mentioned at this stage, that unlike previous attempts to use gas absorption correlations, the proposed model utilizes a continuous linear variation of eddy viscosity near the free surface based on [10]. This is justified by the following facts:

- (i) No measurements of eddy viscosity have yet been obtained in the surface region of freely-falling liquid films.
- (ii) Previous absorption-type eddy profiles fail to justify the extent of the free-surface damping region. Mills & Chung (1973), for example, arbitrarily extend the free-surface damping function until it intersects the Van Driest eddy profile of the solid wall region (see figure 3).
- (iii) Absorption-type eddy profiles assumed a fixed turbulent Schmidt number (defined by the ratio  $\epsilon_M/\epsilon_D$ ,  $\epsilon_D$  being the eddy mass diffusivity) which cannot be justified without experimental data. Furthermore, the available eddy mass-diffusivity studies reveal strong disagreements in the film surface region as shown in figure 6 of Ueda's paper. Nevertheless, the linearized surface profile agrees with Hunt's (1954) work listed in that paper.

### 3. NUMERICAL SOLUTIONS

#### *Velocity field and film thickness*

For a given  $\delta^+$ , the velocity field is obtained by integrating [2] for  $u^+$  as a function of  $y^+$ . The relationship between  $Re$  and  $\delta^+$  is then established by integrating the mass flux across the film:

$$u^+ = \int_0^{y^+} \frac{1 - \frac{y^+}{\delta^+}}{1 + \frac{\epsilon_M}{\nu}} dy^+ \quad [23]$$

and

$$Re = 4 \frac{\Gamma}{\mu} = 4 \int_0^{\delta^+} u^+ dy^+, \quad [24]$$

where  $\Gamma$  is the mass flow rate per unit film width.

Figure 4 shows the functional dependence of  $\beta$  on  $Re$  for isothermal freely-falling water films at 20°C ( $Re_{crit} = 1112$ ). For  $Re > 20 \times 10^3$ , the laminarization parameter becomes negligible due to the vanishing effect of  $Re_{crit}$  on eddy viscosity. The nondimensional thickness  $\beta$  and average film speed  $u_{av}$  in this range could be approximated by the following equations:

$$\beta = \frac{\delta g^{1/3}}{\nu^{2/3}} = \delta^{+2/3} = 0.145 Re^{0.58} \quad [25]$$

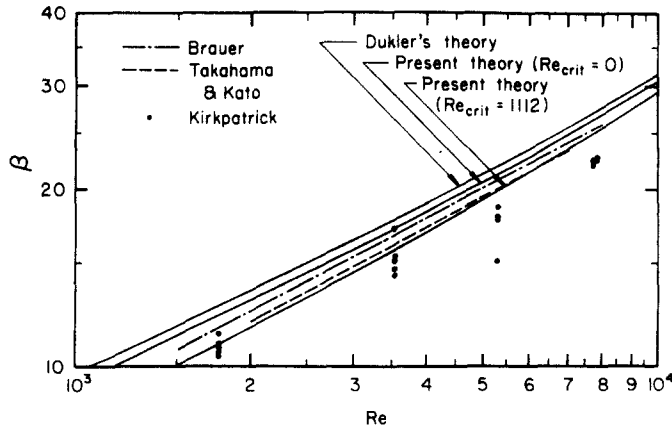


Figure 5. Comparison of calculated film thickness with various theoretical and experimental results in the low-turbulence region.

and

$$\frac{u_{av}}{(vg)^{1/3}} = 1.72 Re^{0.42} \quad [26]$$

The accuracy of the above predictions is tested in figure 4 for vertical water film measurements obtained by various Russian authors. Note that the film thickness variable has the same form used by Gimbutis (1974) for presenting the above data. Figure 5, on the other hand, shows a comparison between our theory and various experimental results in the low Re turbulent range. The theoretical predictions of Dukler (1960) are shown in the same figure for comparison.

Figure 6 shows velocity-profile predictions for freely-falling water films at 20°C ( $Re_{crit} = 1112$ ). Laser-Doppler velocity-profile measurements by Semena & Mel' nichuk (1978) and pitot-probe measurements of Gimbutis *et al.* (1978) are displayed in figure 6 as well. Note that the universal law-of-the-wall velocity profile is approached only for  $Re > 15,000$ .

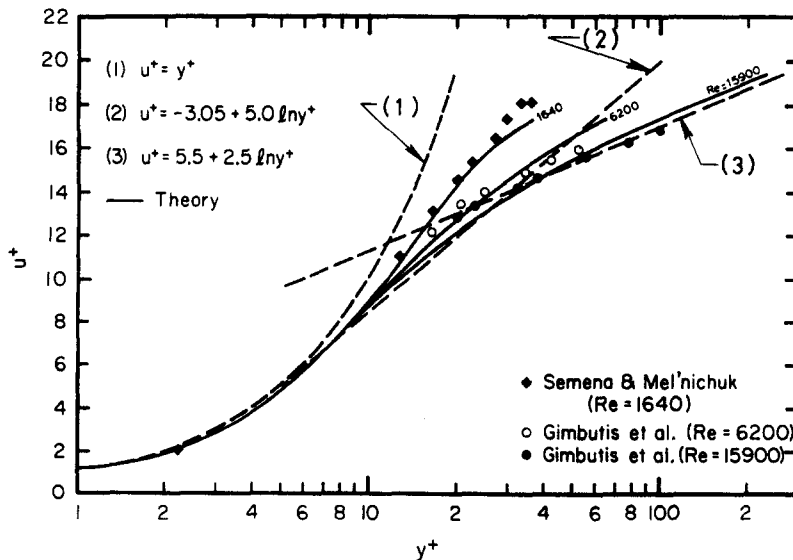


Figure 6. Comparison of calculated and experimental velocity profiles.

*Heat transfer in nonevaporating films*

Fully-developed nonevaporating liquid-film flow is characterized by a uniform temperature profile in the flow direction.

$$\frac{\partial}{\partial x} \left( \frac{T_w - T}{T_w - T_M} \right) = 0, \tag{27}$$

where  $T_w$  is the wall temperature, and  $T_M$  is the mean film temperature defined by

$$T_w - T_M \equiv \frac{\int_0^\delta (T_w - T)u \, dy}{\int_0^\delta u \, dy}. \tag{28}$$

For a constant wall flux,  $(T_w - T_M)$  is uniform with  $x$ . Accordingly,

$$\frac{\partial T}{\partial x} = \frac{dT_w}{dx} = \frac{dT_M}{dx}. \tag{29}$$

Neglecting the axial conduction term in the flow direction, the energy equation reduces to the form:

$$\rho c_p u \frac{dT_M}{dx} = - \frac{dq}{dy}. \tag{30}$$

Based on [3], [28] and [30], the heat transport equations can be nondimensionalized in the following form:

$$\frac{q}{q_w} = 1 - \frac{\int_0^{y^+} u^+ \, dy^+}{\frac{Re}{4}}, \tag{31}$$

$$T^+ = \int_0^{y^+} \frac{\frac{q}{q_w}}{\frac{1}{Pr} + \frac{1}{Pr_T} \cdot \frac{\epsilon_M}{\nu}} \, dy^+ \tag{32}$$

and

$$T_M^+ = \frac{\int_0^{\delta^+} T^+ u^+ \, dy^+}{\frac{Re}{4}}. \tag{33}$$

The integral of [33] can be further simplified through integration by parts. The nondimensional heat transfer coefficients  $h_{HM}^*$  and  $h_{HS}^*$  based on the mean temperature  $T_M$  and the surface temperature  $T_s$ , respectively, could then be presented in the following form:

$$\begin{aligned} h_{HM}^* &\equiv \frac{q_w \nu^{2/3}}{(T_w - T_M) kg^{1/3}} = \frac{\delta^{+1/3} Pr}{T_M^+} \\ &= \frac{\delta^{+1/3} Pr}{\int_0^{\delta^+} \left[ \frac{1 - \frac{\int_0^{y^+} u^+ \, dy^+}{\frac{Re}{4}}}{\frac{1}{Pr} + \frac{1}{Pr_T} \cdot \frac{\epsilon_M}{\nu}} \right] \, dy^+} \end{aligned} \tag{34}$$

and

$$\begin{aligned}
 h_{HS}^* &\equiv \frac{q_w v^{2/3}}{(T_w - T_s) k g^{1/3}} = \frac{\delta^{+1/3} \text{Pr}}{T_s^+} \\
 &= \frac{\delta^{+1/3} \text{Pr}}{1 - \frac{\int_0^{y^+} u^+ dy^+}{\frac{\text{Re}}{4}}}, \\
 &\int_0^{\delta^+} \frac{1}{\frac{1}{\text{Pr}} + \frac{1}{\text{Pr}_T} \cdot \frac{\epsilon_M}{v}}
 \end{aligned} \tag{35}$$

where  $k$  is the thermal conductivity of the liquid.

Since both  $\epsilon_M/v$  and  $\delta^+$  are functions of  $\text{Re}$  and  $\text{Ka}$ , the complete functional dependences of  $T^+$  and  $h^*$  reduce to the following form;

$$T^+ = f(y^+, \text{Re}, \text{Pr}, \text{Ka}), \tag{36}$$

$$h_{HM}^* = f(\text{Re}, \text{Pr}, \text{Ka}) \tag{37}$$

and

$$h_{HS}^* = f(\text{Re}, \text{Pr}, \text{Ka}). \tag{38}$$

Figure 7 shows temperature profiles for freely-falling water films undergoing heating at 20°C ( $\text{Re}_{\text{crit}} = 1112$ ). The plots shown are quite similar to closed-channel-flow profiles because of the weak effect of the free-surface region in the case of heating. Figures 8 and 9 show the variation of  $h_{HM}^*$  and  $h_{HS}^*$  with both  $\text{Re}$  and the average film temperature. Numerical values of  $\text{Pr}$  and  $\text{Ka}$  are given in table 2. Figure 8 illustrates the  $\text{Ka}$  effect on  $h_{HM}^*$  when the laminarization term of [21] is neglected. Notice that this effect vanishes very rapidly beyond  $\text{Re} = 10,000$ . Numerical results could be approximated in this range by the following equations:

$$h_{HM}^* = 0.1 \text{Re}^{0.14} \text{Pr}^{0.35} \tag{39}$$

and

$$h_{HS}^* = 0.069 \text{Re}^{0.16} \text{Pr}^{0.475}. \tag{40}$$

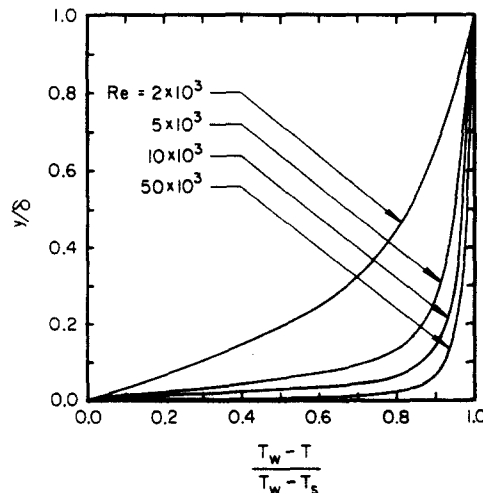


Figure 7. Temperature distribution across heated water films at 20°C.

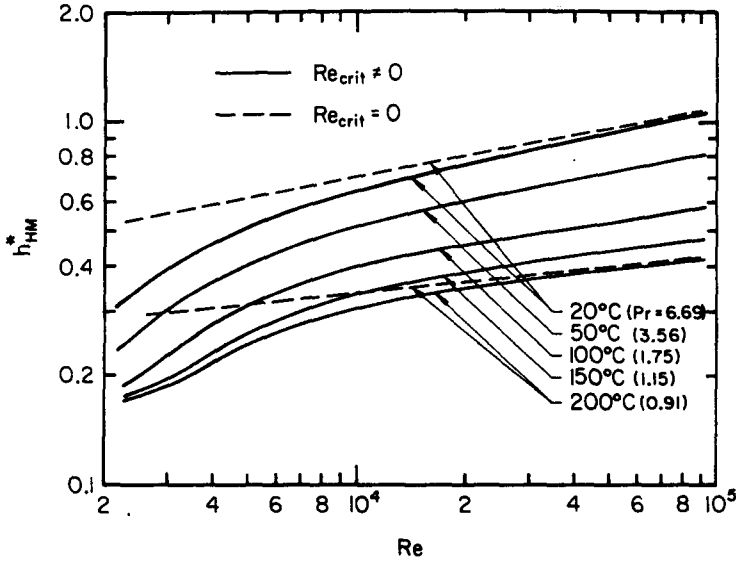


Figure 8. Heat transfer coefficient for heated water films, based on the mean temperature.

Predictions for  $h_{HM}^*$  for freely-falling films are compared in figure 10 with Wilke's (1962) results for water ( $Pr = 5.4, Re_{crit} = 1200$ ), and for a mixture of water and ethylene glycol ( $Pr = 9.4, Re_{crit} = 1000$ ). The coefficients shown have been nondimensionalized according to Wilke's original representation of his data as  $h_{HM}^* \beta_B$ , where  $\beta_B$  is the Brauer (1956) correlation for turbulent-film thickness, given by

$$\beta_B = 0.208 Re^{0.533} \tag{41}$$

As illustrated in figure 10, the agreement between our results and Wilke's measurements is excellent for both fluids. Figure 11 shows another comparison with the data of Gimbutis *et al.* (1978) for a wide range of  $Re$ . Unfortunately, these data were not clearly identified by their respective  $Pr$ . Gimbutis *et al.* stated that their measurements were obtained for freely-falling water films in a temperature range of 15°C ( $Pr = 8.4, Ka = 1.25 \times 10^{-10}$ ) to 40°C ( $Pr = 4.3, Ka = 5.32 \times 10^{-12}$ ). Accordingly, our numerical calculations were carried

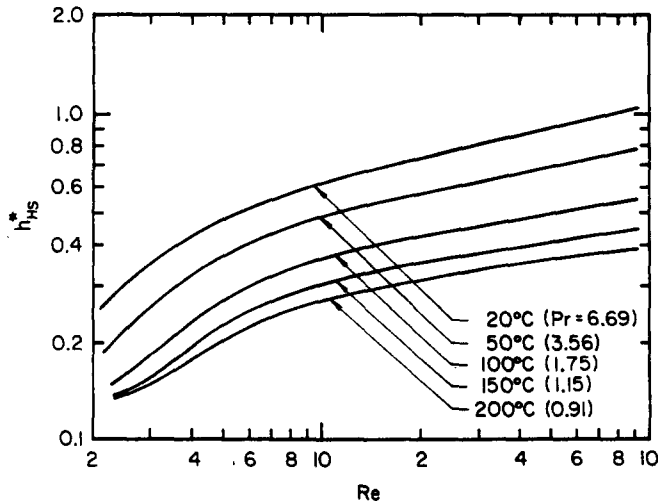


Figure 9. Heat transfer coefficients for heated water films, based on the surface temperature.

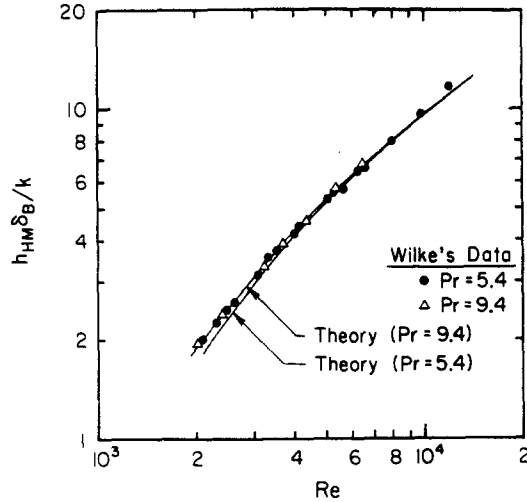


Figure 10. Comparison of calculated heat transfer coefficients with Wilke's data for heated films.

out from an envelope of conditions between the two temperature limits. The comparison shown in figure 11 is based on the variable

$$h_{HM}^* Pr^{-0.34} \left( \frac{Pr_w}{Pr} \right)^{0.25}, \tag{42}$$

recommended by Gimbutis *et al.*, where  $Pr_w$  is evaluated at the wall temperature.

*Heat transfer in evaporating films*

In a fully-developed evaporating (or condensing) film, all the energy supplied at the wall is released at the surface in the form of latent heat. The wall heat flux is thus preserved across the film ( $q = q_w$ ), and the temperature field is obtained directly by integrating [3]:

$$T^+ = \int_0^{y^+} \frac{1}{\frac{1}{Pr} + \frac{1}{Pr_T} \frac{\epsilon_M}{\nu}} dy^+ \tag{43}$$

The nondimensional evaporation heat transfer coefficient  $h_E^*$  is defined in the following manner:

$$h_E^* \equiv \frac{q_w \nu^{2/3}}{(T_w - T_{sat}) kg^{1/3}} = \frac{\delta^{+1/3} Pr}{T_s^+}, \tag{44}$$

where  $T_{sat}$  is the saturation temperature of the liquid.

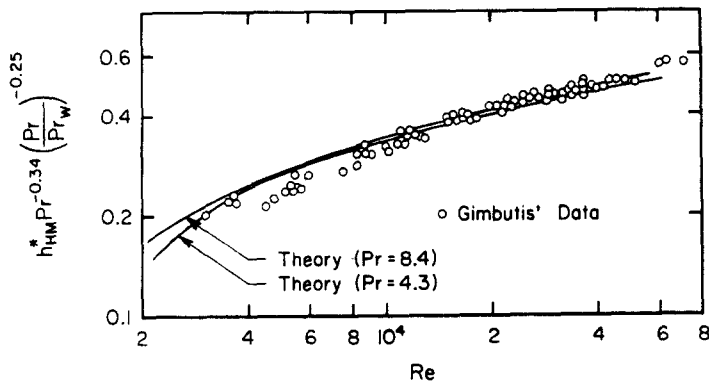


Figure 11. Comparison of calculated heat transfer coefficients with the experimental results of Gimbutis *et al.* for heated water films.

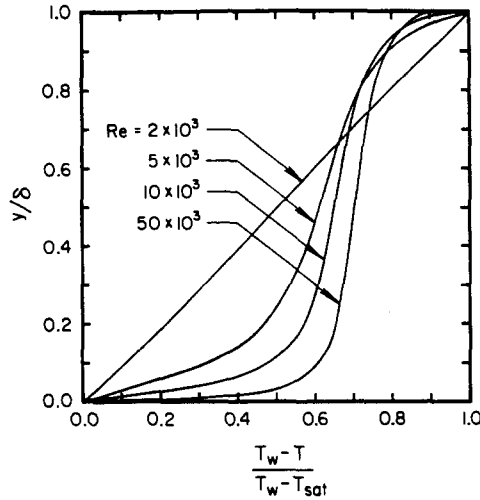


Figure 12. Temperature distribution across evaporating water films at 100°C.

Free-surface activity plays an important role in evaporating liquid films. Since  $\epsilon_M/\nu \rightarrow 0$  at the free surface, the temperature gradient increases significantly in that region, resulting in considerable reduction in the heat transfer coefficient. This fact is clearly demonstrated by the temperature profiles shown in figure 12 for water films at 100°C. These profiles display the uniqueness of evaporating films resulting from the additional thermal boundary layer at the surface.

The functional dependence of  $f_E^*$  for freely-falling films is shown in figure 13. Numerical results are approximated in the fully turbulent range ( $Re > 10^4$ ) by the following equation:

$$h_E^* = 0.042 Re^{0.17} Pr^{0.53} \tag{45}$$

It is interesting to point out that  $h_{HS}^*$  is roughly 50% higher than  $h_E^*$ . This difference is primarily attributed to the laminarization effect of the free-surface region.

Predictions for freely-falling water films are compared in figure 14 with Chun & Seban's (1971) data for two saturation temperatures. Saturated-film measurements by Fujita & Ueda (1976) are also shown. Note that for atmospheric pressure data our numerical results lie between the two independent measurements. For the lower saturation temperature ( $Pr = 5.7$ ) our predictions fall within 7% of the data of Chun & Seban.

According to our previous discussion of the eddy-viscosity model, the best way to check the validity of a particular turbulence model is to compare its numerical predictions with

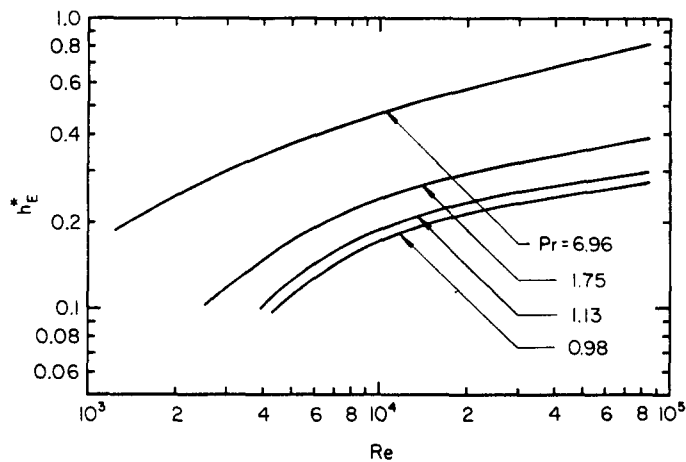


Figure 13. Heat transfer coefficients for evaporating water films.

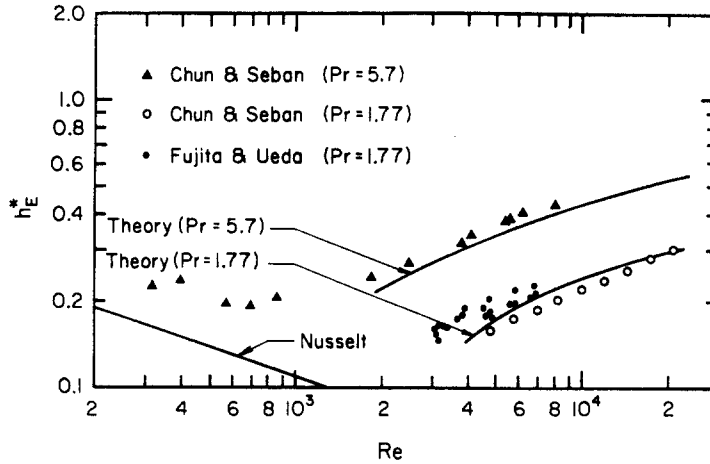


Figure 14. Comparison of calculated heat transfer coefficients and the experimental results.

evaporating liquid-film data. The close agreement exhibited in figure 14 strengthens our confidence in the proposed model.

### CONCLUSIONS

The proposed turbulent-film model exhibits good agreement with experimental data for freely-falling liquid films undergoing heating or evaporation. The model is particularly successful in the low-turbulence region. This was achieved by introducing an empirical correction factor into the fully-developed eddy-viscosity profile. Due to the strong dependence of the heat transfer coefficient on  $Ka$  in the low-turbulence region, the authors believe that generalized correlations based on  $Re$  and  $Pr$  can only be applied to highly turbulent flows ( $Re > 15,000$ ).

*Acknowledgements*—The authors acknowledge the partial support provided by the U.S. Department of Energy (Grant No. DE-FG02-85ER13398) and the MIT Energy Laboratory.

### REFERENCES

- ABBRECHT, P. H. & CHURCHILL, S. W. 1960 The thermal entrance region in fully developed turbulent flow. *AIChE JI* **6**, 268–273.
- BENJAMIN, T. B. 1957 Wave formation in laminar flow down an inclined plane. *J. Fluid Mech.* **2**, 554–561.
- BERBENTE, G. P. & RUCKENSTEIN, E. 1968 Hydrodynamics of wave flow. *AIChE JI* **14**, 772–782.
- BLANGETTI, F. & SCHLUNDER, E. U. 1978 Local heat transfer coefficients on condensation in a vertical tube. *Proc. 6th Int. Heat Transfer Conf.* **2**, 437–442.
- BRAUER, H. 1956 Stromung und warmenbergang bei rieselfilmen. *VDI Forsch Hft.* **457**.
- BRUMFIELD, L. K. & THEOFANOUS, T. G. (1976) On the prediction of heat transfer across trubulent liquid films. *J. Heat Transfer* **98**, 496–502.
- CHU, K. J. & DUKLER, A. E. 1974 Statistical characteristics of thin, wavy films: Part II. Studies of the substrate and its wave structure. *AIChE JI* **20**, 695–706.
- CHUN, K. R. & SEBAN R. A. 1971 Heat transfer to evaporating liquid films. *J. Heat Transfer* **93**, 391–396.
- CHUNG, D. K. 1974 An experimental investigation of gas absorption into a turbulent liquid film with interfacial shear. Ph.D. Thesis, UCLA, Los Angeles, Calif.

- CHUNG, D. K. & MILLS, A. F. 1974 Effects of interfacial shear and gas absorption into a turbulent falling film with concurrent gas flow. *Lett. Heat Mass Transfer* **1**, 43–48.
- DUKLER, A. E. 1960 Fluid mechanics and heat transfer in vertical falling-film systems. *Chem. Engng Prog.* **56**, 1–10.
- FEIND, K. 1960 Stromungsmunstersuchungen bei gegenstrom von rieselfilmen und gas in lotrechten rohren. *VDI Forsch Hft.* **481**.
- FUJITA, T. & UEDA, T. 1976 Heat transfer to falling liquid films and film breakdown—II. *Int. J. Heat Mass Transfer* **21**, 109–118.
- GIMBUTIS, G. 1974 Heat transfer of a turbulent falling film. *Proc. 5th Int. Heat Transfer Conf.* **2**, 85–89.
- GIMBUTIS, G. J., DROBAVICIUS, A. J. & SINKUNAS, S. S. 1978 Heat transfer of a turbulent water film at different initial flow conditions and high temperature gradients. *Proc. 6th Int. Heat Transfer Conf.* **1**, 321–326.
- GOLLAN, A. & SIDEMAN, S. 1969 On the wave characteristics of falling films. *AIChE Jl.* **15**, 301–303.
- HABIB, I. & NA, T. 1974 Prediction of heat transfer in turbulent pipe flow with constant wall temperature. *J. Heat Transfer* **96**, 253–254.
- HANRATTY, T. J. & HERSHMAN, A. 1961 Initiation of roll waves. *AIChE Jl* **7**, 488–497.
- HUBBARD, G. L., MILLS, A. F. & CHUNG, D. K. 1976 Heat transfer across a turbulent falling film with concurrent vapour flow. *J. Heat Transfer* **98**, 319–320.
- HUNT, J. N. 1954 The turbulent transport of suspended sediment in open channels. *Proc. R. Soc.* **A224**, 322–335.
- IRIBARNE, A., GOSMAN, A. D. & SPALDING, D. B. 1967 A theoretical and experimental investigation of diffusion-controlled electrolytic mass transfer between a falling film and a wall. *Int. J. Heat Mass Transfer* **10**, 1661–1676.
- KAPITZA, P. L. 1965 *Collected Papers by P. L. Kapitza*, Vol. 2. Pergamon Press, New York.
- KAYS, W. M. 1972 Heat transfer to the transpired turbulent boundary layer. *Int. J. Heat Mass Transfer* **15**, 1023–1044.
- KAYS, W. M. & CRAWFORD, M. E. 1980 *Convective Heat and Mass Transfer*, 2nd edn. McGraw-Hill, New York.
- KIRKPATRICK, A. T. 1980 Wave mechanics of inclined and rotating liquid films. Ph.D. Thesis, MIT, Cambridge, Mass.
- KUNZ H. R. & YERAZUNIS, S. 1967 An analysis of film condensation, film evaporation and single-phase heat transfer. ASME Paper No. 67-HT-1.
- LAMOURELLE, A. P. & SANDALL, O. C. 1972 Gas absorption into a turbulent liquid. *Chem. Engng. Sci.* **27**, 1035–1043.
- LEE, J. 1964 Turbulent film condensation. *AIChE Jl* **10**, 540–544.
- LIMBERG, H. 1973 Wärmeübergang an turbulente und laminare rieselfilme. *Int. J. Heat Mass Transfer* **16**, 1691–1702.
- MASSOT, C., IRANI, F. & LIGHTFOOT, E. N. 1966 Modified description of wave motion in a falling film. *AIChE Jl* **12**, 445–455.
- MILLS, A. F. & CHUNG, D. K. 1973 Heat transfer across turbulent falling films. *Int. J. Heat. Mass Transfer* **16**, 694–696.
- NUSSELT, N. 1916 Die oberflächenkondensation des wasserdampfes. *Z. Ver. dt. Ing.* **60**, 541–569.
- PORTALSKI, S. 1963 Studies of falling liquid film flow: film thickness on a smooth vertical plate. *Chem. Engng Sci.* **18**, 787–804.
- PORTALSKI, S. & CLEGG, A. J. 1972 An experimental study of wave inception on falling liquid films. *Chem. Engng* **27**, 1257–1265.
- ROHSENOW, W. M., WEBBER, J. H. & LING, A. T. 1956 Effect of vapour velocity on laminar and turbulent film condensation. *Trans. ASME* **78**, 1637–1643.
- SALAZAR, R. P. & MARSCHALL, E. 1978 Time-averaged local thickness measurements in falling liquid film flow. *Int. J. Multiphase Flow* **4**, 405–412.
- SEBAN, R. A. 1954 Remarks on film condensation with turbulent flow. *Trans. ASME* **76**, 299–303.

- SEBAN, R. A. & FAGHRI, A. 1976 Evaporation and heating with turbulent falling liquid films. *J. Heat Transfer* **98**, 315–318.
- SEMENA, M. G. & MEL'NICHUK, G. A. 1978 Mean-velocity distributions in a falling film. *Fluid Mech. Sov. Res.* **7**, 145–151.
- SKELLAND, A. H. P. & POPADIC, V. O. 1975 Pseudoplastic falling films with concurrent gas streams. *AIChE JI* **21**, 861–865.
- SPALDING, D. B. 1961 A single formula for the law of the wall. *J. appl. Mech.* **83**, 455–458.
- TAKAHAMA, H. & KATO, S. 1980 Longitudinal flow characteristics of vertically falling liquid films without concurrent gas flow. *Int J. Multiphase Flow* **6**, 203–215.
- UEDA, H., MOLLER, R., KOMORI, S. & MIZUSHIMA, T. 1977 Eddy diffusivity near the free surface of open channel flow. *Int. J. Heat Mass Transfer* **20**, 1127–1136.
- VAN DRIEST, E. R. 1956 On turbulent flow near a wall. *J. aerosp. Sci.* **23**, 1007–1011.
- WHITAKER, S. 1964 Effect of surface active agents on the stability of falling liquid films. *Ind. Engng Chem. Fundam.* **3**, 132–141.
- WILKE, W. 1962 Wärmeübergang an rieselfilme. *VDI Forsch Hft.* **490**.
- YIH, S. M. & CHEN, C. H. 1982 Heat transfer in the thermal entrance region of a turbulent falling liquid film undergoing heat or evaporation. *Proc. 7th Int. Heat Transfer Conf.* **3**, 125–130.